Molecular Therapy
Nucleic Acids
Original Article

Development of versatile allele-specific siRNAs able to silence all the dominant dynamin 2 mutations

Swati Dudhal,[1,2] Lylia Mekzine,[1,2] Bernard Prudhon,[1] Karishma Soocheta,[1] Bruno Cadot,[1] Kamel Mamchaoui,[1] Delphine Trochet,[1,3] and Marc Bitoun[1,3]

[1]Sorbonne Université, Inserm, Institut de Myologie, Centre de Recherche en Myologie, 75013 Paris, France

Dominant centronuclear myopathy (CNM) is a rare form of congenital myopathy associated with a wide clinical spectrum, from severe neonatal to milder adult forms. There is no available treatment for this disease due to heterozygous mutations in the *DNM2* gene encoding Dynamin 2 (DNM2). Dominant *DNM2* mutations also cause rare forms of Charcot-Marie-Tooth disease and hereditary spastic paraplegia, and deleterious DNM2 overexpression was noticed in several diseases. The proof of concept for therapy by allele-specific RNA interference devoted to silence the mutated mRNA without affecting the normal allele was previously achieved in a mouse model and patient-derived cells, both expressing the most frequent *DNM2* mutation in CNM. In order to have versatile small interfering RNAs (siRNAs) usable regardless of the mutation, we have developed allele-specific siRNAs against two non-pathogenic single-nucleotide polymorphisms (SNPs) frequently heterozygous in the population. In addition, allele-specific siRNAs against the p.S619L DNM2 mutation, a mutation frequently associated with severe neonatal cases, were developed. The beneficial effects of these new siRNAs are reported for a panel of defects occurring in patient-derived cell lines. The development of these new molecules allows targeting the large majority of the patients harboring *DNM2* mutations or overexpression by only a few siRNAs.

INTRODUCTION

Autosomal dominant centronuclear myopathy (AD-CNM; OMIM: #160150) is a rare congenital myopathy associated with a wide clinical spectrum from severe-neonatal to mild-adult forms.[1] The classical late-childhood or adult-onset form exhibits delayed motor milestones and diffuse skeletal muscle weakness mainly involving facial and limb muscles, whereas pediatric patients affected by the severe neonatal form usually have generalized weakness, hypotonia, and facial weakness.[2,3] AD-CNM results from mutations in the *DNM2* gene (OMIM: *602378, which encodes dynamin 2 (DNM2).[4] In addition, *DNM2* mutations also cause rare forms of Charcot-Marie-Tooth disease (CMT, OMIM: #606482)[5] and hereditary spastic paraplegia (HSP),[6] and a deleterious DNM2 overexpression was reported in several cancers[7–12] and the X-linked recessive CNM,[13] highlighting a large DNM2 involvement in human diseases. DNM2 belongs to the superfamily of large GTPases[14] acting as a mechanochemical scaffolding molecule that oligomerizes and deforms biological membranes leading to the formation and release of vesicles from the plasma membrane and intracellular membrane compartments. Furthermore, several studies have highlighted the role of DNM2 as a regulator of both actin and microtubule cytoskeletons.[15,16] More than 30 *DNM2* mutations have been reported in AD-CNM patients[17] and, when tested, the mutant protein is normally expressed.[4,18] Mutations are thought to be responsible for a gain-of-function and/or a dominant-negative effect through increased GTPase activity and formation of abnormal stable DNM2 oligomers.[19,20] In addition, absence of haploinsufficiency in AD-CNM is supported by data from patients and absence of phenotype developed by heterozygous (HTZ) knockout mice expressing 50% *Dnm2*.[13,21]

We recently developed a therapeutic approach for the *DNM2*-related AD-CNM by allele-specific RNA interference (AS-RNAi) devoted to specifically suppressing the expression of the mutated protein from the mutated allele without reducing expression from the wild-type (WT) allele.[22] AS-RNAi was demonstrated as a powerful strategy in cells from patients and animal models of numerous dominant inherited diseases[23] and led to two clinical trials targeting a Keratin 6a mutation causing Pachyonychia congenita[24] and one mutation of the *KRAS* gene involved in pancreatic cancer.[25] By applying this strategy, we reported functional rescue in the Knock-In-*Dnm2*$^{R465W/+}$ mouse model of AD-CNM and patient-derived fibroblasts, both expressing the most frequent mutation encountered in patients (p.R465W found in around 30% of patients).[22] Extending this strategy to the entire AD-CNM patient population requires either to

Received 28 March 2022; accepted 10 August 2022;
https://doi.org/10.1016/j.omtn.2022.08.016.

[2]These authors contributed equally

[3]These authors contributed equally

Correspondence: Delphine Trochet, Sorbonne Université, Inserm, Institut de Myologie, Centre de Recherche en Myologie, 75013 Paris, France.
E-mail: d.trochet@institut-myologie.org
Correspondence: Marc Bitoun, Sorbonne Université, Inserm, Institut de Myologie, Centre de Recherche en Myologie, 75013 Paris, France.
E-mail: m.bitoun@institut-myologie.org

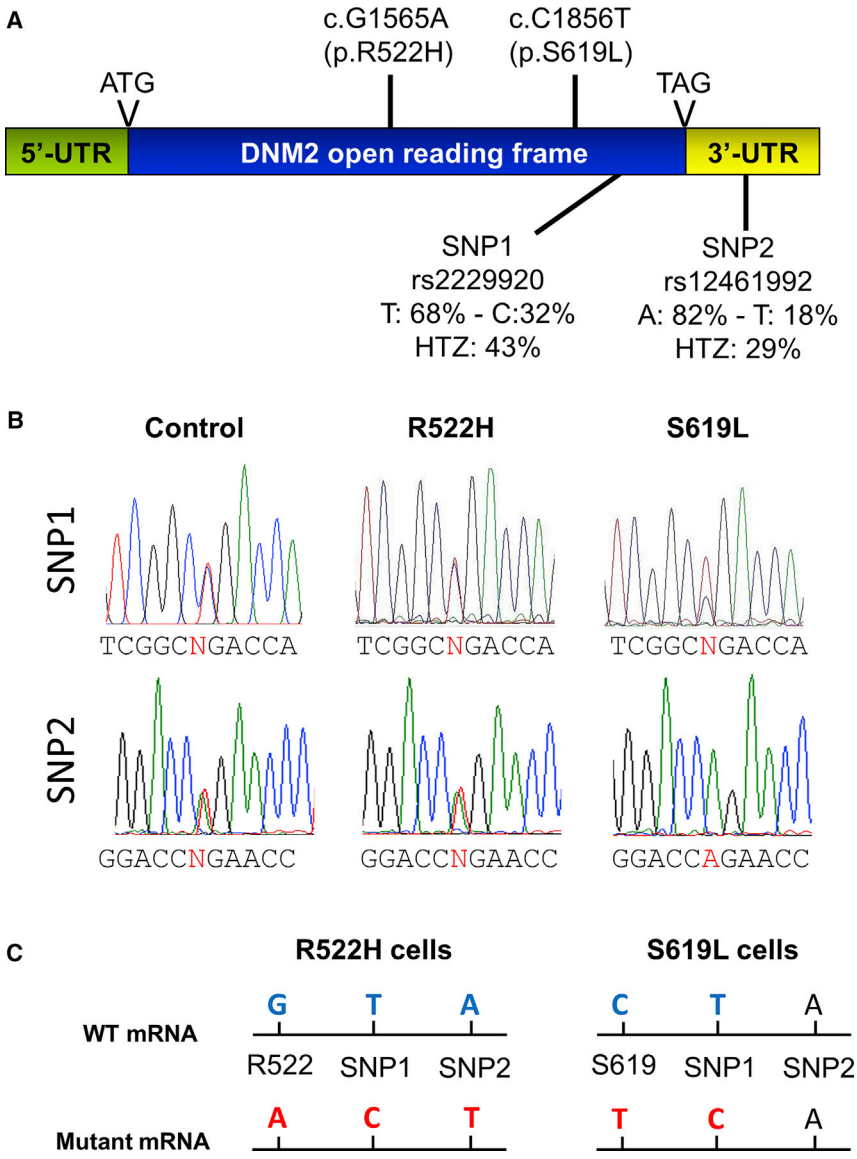

Figure 1. Identification of targetable SNPs and heterozygous cells

(A) Schematic representation of the *DNM2* mRNA showing the location of two CNM mutations and two single-nucleotide polymorphisms (SNPs). For each SNP, the frequencies of the two alleles are indicated, as well as the frequency of heterozygosity in the population. (B) Sequencing of the SNPs in healthy control and two patient-derived cell lines. (C) Results of the genotyping of SNP1 and SNP2 on the wild-type (WT) and mutated *DNM2* mRNAs in the two patient-derived cell lines. HTZ, heterozygous.

develop personalized medicine through specific small interfering RNA (siRNA) for each reported mutation or to develop an alternative approach allowing to target the distinct dominant *DNM2* mutations using a limited number of allele-specific siRNAs. In particular cases of triplet repeat diseases such as Huntington's disease or spinocerebellar ataxia in which the sequence of the genetic mutations makes allele-specific silencing challenging, AS-siRNAs have been developed against disease-associated single-nucleotide polymorphisms (SNPs).[23,26–28] We took advantage of the presence in the *DNM2* sequence of two non-pathogenic SNPs frequently HTZ in the general population to develop a similar strategy for the AD-CNM. Here, we report the identification of effective AS-siRNA against the two nucleotide versions of the two non-pathogenic *DNM2* SNPs, which may be used to silence any mutation carried by the same mRNA. In addition, the first AS-siRNAs targeting a *DNM2* mutation associated with severe neonatal phenotype, i.e., the p.S619L mutation, have been developed. We also report the functional benefits of this new set of siRNAs on several defects identified in patient-derived cell lines. The development of these new AS-siRNAs, in addition to the previous ones against the p.R465W mutation, provides a panoply of allele-specific molecules able to target the large majority of AD-CNM patients. Interestingly, siRNAs against the *DNM2* SNPs represent versatile molecules with larger potential applications to silence *DNM2* mutations in CMT and HSP and to reduce DNM2 expression in a controlled manner in diseases associated with deleterious overexpression.

RESULTS

Identification of targetable SNPs and HTZ cells

We performed an *in silico* analysis devoted to identifying *DNM2* SNPs exhibiting the highest frequency of heterozygosity in human. We looked in the Ensembl Genome Browser (https://www.ensembl.org; human genome assembly GRCh38.p13) for synonymous variants in the *DNM2* open reading frame or variants in the 5′- and -3′ untranslated transcribed regions (UTRs) exhibiting a frequency of the second most common allele between 0.1 and 0.5 in the general population. Using these criteria, we identified two SNPs (Figure 1A). The first SNP was a T/C variation (rs2229920, thereafter called SNP1) identified as a synonymous variant of the alanine 713 (c.2139T>C, NM_001005361.3) of the DNM2 protein. Allele frequencies for SNP1 were determined at 0.688 for the allele T and 0.321 for the allele C on 250,390 counts (gnomAD exomes r2.1.1) resulting in a theoretical HTZ frequency of 0.43 (calculated as 2 × frequency of T allele × frequency of C allele). In agreement, PCR and Sanger sequencing in a cohort of 52 CNM patients identified 42.3% of SNP1 heterozygosity. The second SNP was an A/T variation (rs12461992, thereafter called SNP2) identified as a 3′ UTR variant located 268 nt after the stop codon (*268A>T, NM_001005361.3). Allele frequencies for SNP2 were determined at 0.824 for allele A

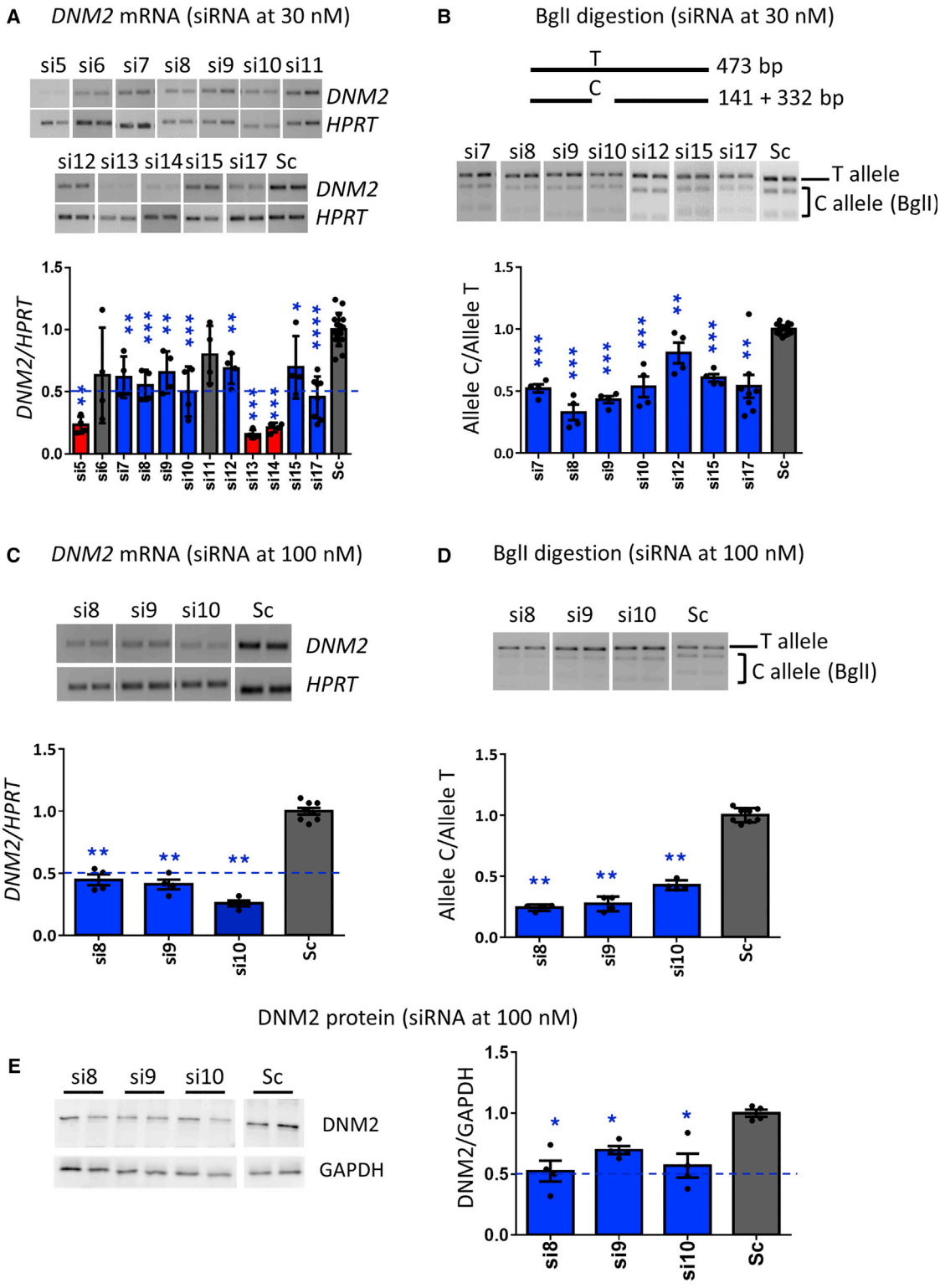

Figure 2. Identification of allele-specific siRNA against the C version of SNP1

(A) Expression of the *DNM2* mRNA 48 h after siRNA transfection at 30 nM. Agarose gel electrophoresis of *DNM2* and *HPRT* RT-PCR products and quantification of *DNM2* expression normalized to *HPRT* (n ≥ 4 per condition). (B) BglI digestion profile on the *DNM2* PCR product including the SNP1 sequence and quantification of the C/T ratio

(legend continued on next page)

and 0.176 for allele T, resulting in a theoretical HTZ frequency of 0.29 on 143,008 counts (gnomAD exomes r3.0), and 23% of SNP2 heterozygosity was found in our cohort of patients. No clinical sign was associated with SNP1 and SNP2.

We next thought to identify cells harboring the SNPs at HTZ state that were required to screen for allele-specific siRNA against the SNPs. RT-PCR products encompassing the SNPs were amplified from fibroblast cell lines from two healthy control subjects and two CNM patients. Sanger sequencing of these RT-PCR products led to identifying one healthy control cell line HTZ for the two SNPs, one CNM cell line (p.R522H DNM2 mutation) harboring the two SNPs at HTZ state, and one CNM cell line (p.S619L DNM2 mutation) harboring only the SNP1 at HTZ state (Figure 1B). Through RT-PCR, cloning, and Sanger sequencing of a single allele, we determined that in the R522H cell line, the mutated mRNA also harbored the C version of SNP1 and T version of SNP2, and that in the S619L cell line, the mutated mRNA harbored the C version of SNP1 (Figure 1C). Altogether, we identified two SNPs targetable by AS-RNAi, one healthy control cell line to perform the siRNA screening, and two patient-derived cell lines for the functional evaluation of the identified AS-siRNA.

Allele-specific siRNA against the C allele of SNP1

For all the screening for allele-specific siRNAs against SNP1 and SNP2 reported in this study, we used one healthy control cell line and looked for allele-specific siRNA leading to around 50% expression of DNM2 mRNA and protein as a result of specific silencing of the targeted allele. We first thought to identify AS-siRNA against the C version of the SNP1 (Figures 2 and S1). Twelve 19-nt siRNAs carrying a single mismatch with the untargeted T version on the positions 5–17 (called si5–si17) were assessed. At low concentration (30 nM), si6 and si11 were not able to significantly reduce *DNM2* mRNA expression compared with scramble siRNA-transfected cells (Figure 2A). In addition, si5, si13, and si14 led to an excessive reduction of *DNM2* transcript relative to the expected 50%, and seven siRNAs (si7, si8, si9, si10, si12, si15, and si17) reduced the *DNM2* expression in the expected range (Figure 2A). RT-PCR and BglI restriction enzyme digestion assay was used to discriminate the C (digested) from the T (undigested) alleles of SNP1 (Figure S2A). The seven siRNAs reduced the C/T ratio compared with scramble siRNA (Figure 2B) with the lower ratio reached by si8 and si9. Quantification of each allele relative to *HPRT* mRNA showed that si8, si9, and si10 reduced expression of the allele C without affecting the T (Figure S1A). At the same concentration, si8, si9, and si10 also reduced expression of the DNM2 protein around the expected 50% compared with scramble siRNA in western blot (Figure S1B). The maintenance of allele specificity at higher concentration (100 nM) was then assessed for si8, si9, and si10. The three siRNAs reduced total *DNM2* mRNA content and close to the expected 50% decrease for si8 and si9 (Figure 2C). Allele specificity of si8 and si9 against the targeted C allele was maintained as demonstrated by the C/T ratio reduction (Figure 2D) and confirmed by quantification of each allele relative to *HPRT* expression (Figure S1C). Maintenance of efficacy and allele specificity of si8 and si9 at higher concentration was also demonstrated on DNM2 protein by western blot showing a significant decrease in DNM2 protein content that did not exceed 50% (Figure 2E). Altogether, these data validate si8 and si9 as the best allele-specific siRNAs against the C version of the SNP1.

Allele-specific siRNA against the T allele of the SNP1

To identify AS-siRNA against the T version of SNP1, we assessed siRNA with mismatches at positions 8, 9, and 10, relative to the untargeted C allele in agreement with our previous screening. At low concentration (30 nM), si8 and si9 significantly reduced the *DNM2* expression in the expected range (Figure 3A). The RT-PCR assay and BglI digestion used to distinguish the targeted T allele from the untargeted C allele showed that the three siRNAs significantly reduced the T/C ratio compared with scramble siRNAs (Figures 3B and S3A). Notably, an increase in the untargeted allele C was observed with si9 (Figure S3A, right panel), suggestive of a genetic regulation promoting the expression of the untargeted allele. At this concentration, the DNM2 protein content was not changed with these three siRNAs (Figure S3B). At higher concentration (100 nM), the total *DNM2* mRNA amount was reduced for the three siRNAs remaining close to the 50% threshold for si8 and si9 (Figure 3C), and allele specificity of the three siRNAs against the targeted T allele was maintained as demonstrated by the T/C ratio reduction (Figure 3D) and the quantification of each allele relative to *HPRT* expression (Figure S3C). A significant increase in the untargeted allele was still observed (Figure S3C, right panel) for si9 and si10. At this concentration, western blot showed a significant decrease in DNM2 protein content for si8, si9, and si10 compared with scramble siRNAs (Figure 3E). Altogether, these data validate si8 and si9 as allele-specific siRNAs against the T version of the SNP1.

Allele-specific siRNA against the T allele of SNP2

To screen for AS-siRNA against the T version of SNP2, we assessed 12 siRNAs carrying a mismatch with the untargeted A allele from positions 6–17 (Figures 4 and S4). Transfected at 30 nM for 48 h, si11, si12, si13, si14, si15, si16, and si17 reduced *DNM2* mRNA expression compared with scramble siRNA-transfected cells, and with the exception of si14 and si15, they all led to a reduction close to 50% (Figure 4A). RT-PCR and Psp5II restriction enzyme digestion assay was used to discriminate the T digested allele from the A undigested allele (Figures 4B and S1). Using this assay, we showed that the lower

($n \geq 4$ per condition) after transfection with siRNA at 30 nM. (C) Expression of the *DNM2* mRNA 48 h after siRNA transfection at 100 nM. Agarose gel electrophoresis of *DNM2* and *HPRT* RT-PCR products and quantification of *DNM2* expression normalized to *HPRT* ($n \geq 4$ per condition). (D) BglI digestion profile on the *DNM2* PCR product including the SNP1 sequence and quantification of the C/T ratio ($n \geq 4$ per condition) after transfection with siRNA at 100 nM. (E) DNM2 western blot and quantification of the signal by densitometry after siRNA transfection at 100 nM concentration. GAPDH was used as a loading control ($n \geq 4$). Data information: in scatterplots, the bars are mean values and error bars indicate SEM. ****$p < 0.0001$, ***$p < 0.001$, **$p < 0.01$, *$p < 0.5$ using a two-tailed Mann-Whitney *U* test relative to the scramble siRNA (Sc).

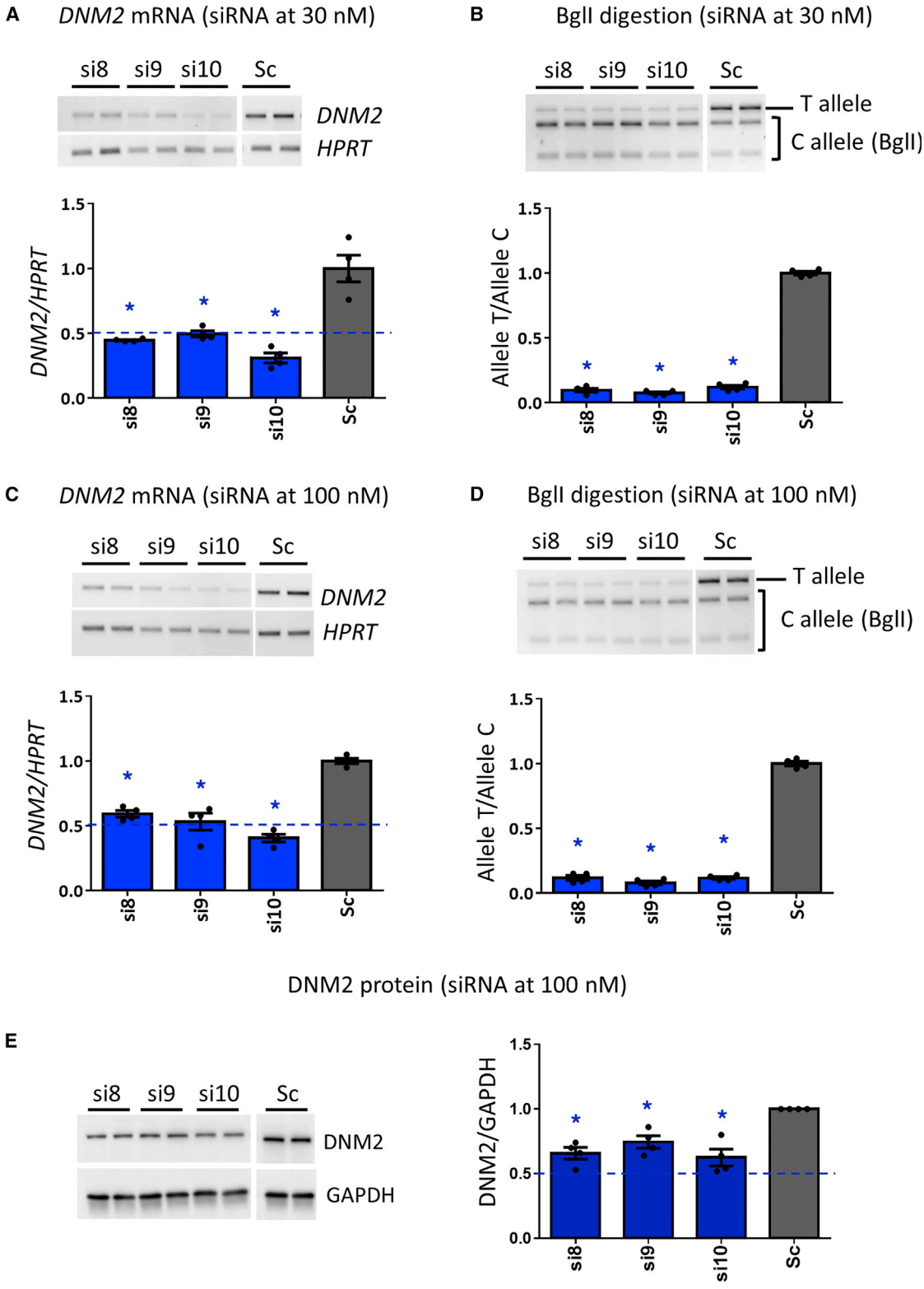

(legend on next page)

T/A ratio compared with scramble siRNA was reached by si11, si16, and si17 (Figure 4B). Quantification of each allele relative to *HPRT* mRNA showed that the reduced T/A ratio resulted from a decrease in the expression of the T allele without reducing the A (Figure S4A). For si17, a significant increase in the A allele was also noticed (Figure S4A, right panel). At this low concentration, only si11 and si16 reduced expression of the DNM2 protein around the expected 50% when compared with scramble siRNA (Figure S4B). We next assessed the maintenance of allele specificity for si11, si16, and si17 at higher concentration (100 nM). Semi-quantitative RT-PCR showed a significant reduction of around 50% of total *DNM2* mRNA for each siRNA (Figure 4C). The three siRNAs reduced the T/A ratio compared with scramble siRNA (Figure 4D) through a specific impact on the T allele for si11 and si16 (Figure S4C). At this higher concentration, DNM2 protein content did not exceed 50% (Figure 4E). Altogether, these data validate si11 and si16 as efficient allele-specific siRNA against the T version of the SNP2.

Allele-specific siRNA against the A allele of SNP2

Previous results on the T allele of SNP2 showed a large number of mismatch positions in the siRNAs efficient to develop AS-siRNA. Consequently, we started the screening for AS-siRNA against the A allele by introducing one mismatch in the central region of the siRNA (positions 9–11) frequently shown with the highest specificity in previously reported studies (Figures 5 and S5).[23] At a low concentration (30 nM), si9, si10, and si11 significantly reduced the DNM2 expression in the expected 50% range (Figure 5A). The RT-PCR assay and Psp5II digestion used to distinguish the targeted A allele from the untargeted T allele showed that the three siRNAs significantly reduced the A/T ratio compared with scramble siRNA through the highest impact on the A allele for si9 and si11 (Figures 5B and S5A). At this concentration, the DNM2 protein content was significantly reduced with si10 and si11 (Figure S5B). At higher concentration (100 nM), a significant reduction of total *DNM2* mRNA was observed for the three siRNAs (Figure 5C), and Psp5II digestion of the RT-PCR products showed maintenance of allele specificity (Figure 5D). Quantification of each allele relative to *HPRT* expression showed a reduction of the A allele using si9 and si11 and an upregulation of the untargeted allele T with the three siRNAs (Figure S5C). At this concentration, DNM2 protein content, quantified by western blot, was reduced by si10 and si11 (Figure 5E), but not by si9, probably because of the upregulation of the untargeted T allele (Figure S5C). Altogether, these data validate si11 as the most efficient allele-specific siRNA against the A version of the SNP2.

Allele-specific siRNA against the p.S619L DNM2 mutation

In order to compare the functional benefit of siRNA directed against the SNPs or a mutation, we screened for AS-siRNA against the p.S619L (c.C1856T) (Figures 6 and S6). The S619L patient-derived fibroblasts were used to screen for 15 siRNAs (si3–si17) named depending on the position of the mismatch with the WT sequence of the *DNM2* mRNA. At low concentration (30 nM), si9 and si11 were not able to significantly reduce *DNM2* mRNA expression compared with scramble siRNA, and si4, si5, si7, and si16 led to an excessive reduction of *DNM2* transcript relative to the 50% expected (Figure 6A). Nine siRNAs (si3, si6, si8, si10, si12, si13, si14, si15, and si17) significantly reduced the *DNM2* expression, and among them, si6, si8, si10, si13, si15, and si17 reduced the mRNA amount in the expected range around 50% (Figure 6A). Given that the S619L mutation does not introduce or remove a restriction site relative to the WT sequence, we used the presence of the SNP1 at the HTZ state in this patient cell line to quantify allele specificity of the nine siRNAs using BglI digestion of the SNP1 sequence (the C allele of SNP1 and the *DNM2* mutation carried by the same mRNA; Figures 1C and S7B). The nine siRNAs significantly reduced the C/T (i.e., the mutant/WT) ratio compared with scramble siRNA (Figure 6B), with the lower ratio reached by si10. Quantification of each allele relative to *HPRT* mRNA showed that the nine siRNAs reduced expression of the mutated allele, with some of them inducing increased expression in the WT allele (Figure S6A). We assessed the impact on the DNM2 protein content of 4 siRNAs of the 15 (si6, si8, si10, and si13) and showed a significant reduction that did not exceed 50% for the 4 siRNAs (Figure S6B). At a higher concentration (100 nM), a significant reduction of total *DNM2* mRNA was observed for the four siRNAs (Figure 6C), and allele specificity was maintained (Figures 6D and S6C) with the maximum impact on the mutated mRNA reached with si10. At this concentration, DNM2 protein content, quantified by western blot, was significantly reduced by the four siRNAs, and the decrease did not exceed 50% (Figure 6E). Altogether, these data validate four allele-specific siRNAs (si6, si8, si10, and si13) against the S619L DNM2 mutant allele.

Rescue of clathrin-mediated endocytosis and cell surface by AS-siRNA

DNM2 is well recognized for its role in endocytosis, and the defect of clathrin-mediated endocytosis (CME) was previously demonstrated in AD-CNM patient-derived fibroblasts.[18,29] We assessed CME through fluorescent transferrin uptake measurement in the healthy control and the two DNM2-CNM fibroblast cell lines. Under basal conditions, CME was decreased in fibroblasts harboring the R522H

Figure 3. Identification of allele-specific siRNA against the T version of SNP1

(A) Expression of the *DNM2* mRNA 48 h after siRNA transfection at 30 nM. Agarose gel electrophoresis of *DNM2* and *HPRT* RT-PCR products and quantification of *DNM2* expression normalized to *HPRT* ($n \geq 4$ per condition). (B) BglI digestion profile on the *DNM2* PCR product including the SNP1 sequence and quantification of the T/C ratio ($n \geq 4$ per condition) after transfection with siRNA at 30 nM. (C) Expression of the *DNM2* mRNA 48 h after siRNA transfection at 100 nM. Agarose gel electrophoresis of *DNM2* and *HPRT* RT-PCR products and quantification of *DNM2* expression normalized to *HPRT* ($n \geq 4$ per condition). (D) BglI digestion profile on the *DNM2* PCR product including the SNP1 sequence and quantification of the T/C ratio ($n \geq 4$ per condition) after transfection with siRNA at 100 nM. (E) DNM2 western blot and quantification of the signal by densitometry after siRNA transfection at 100 nM concentration. GAPDH was used as a loading control ($n \geq 4$). Data information: in scatterplots, the bars are mean values and error bars indicate SEM. *$p < 0.5$ using a two-tailed Mann-Whitney *U* test relative to the scramble siRNA (Sc).

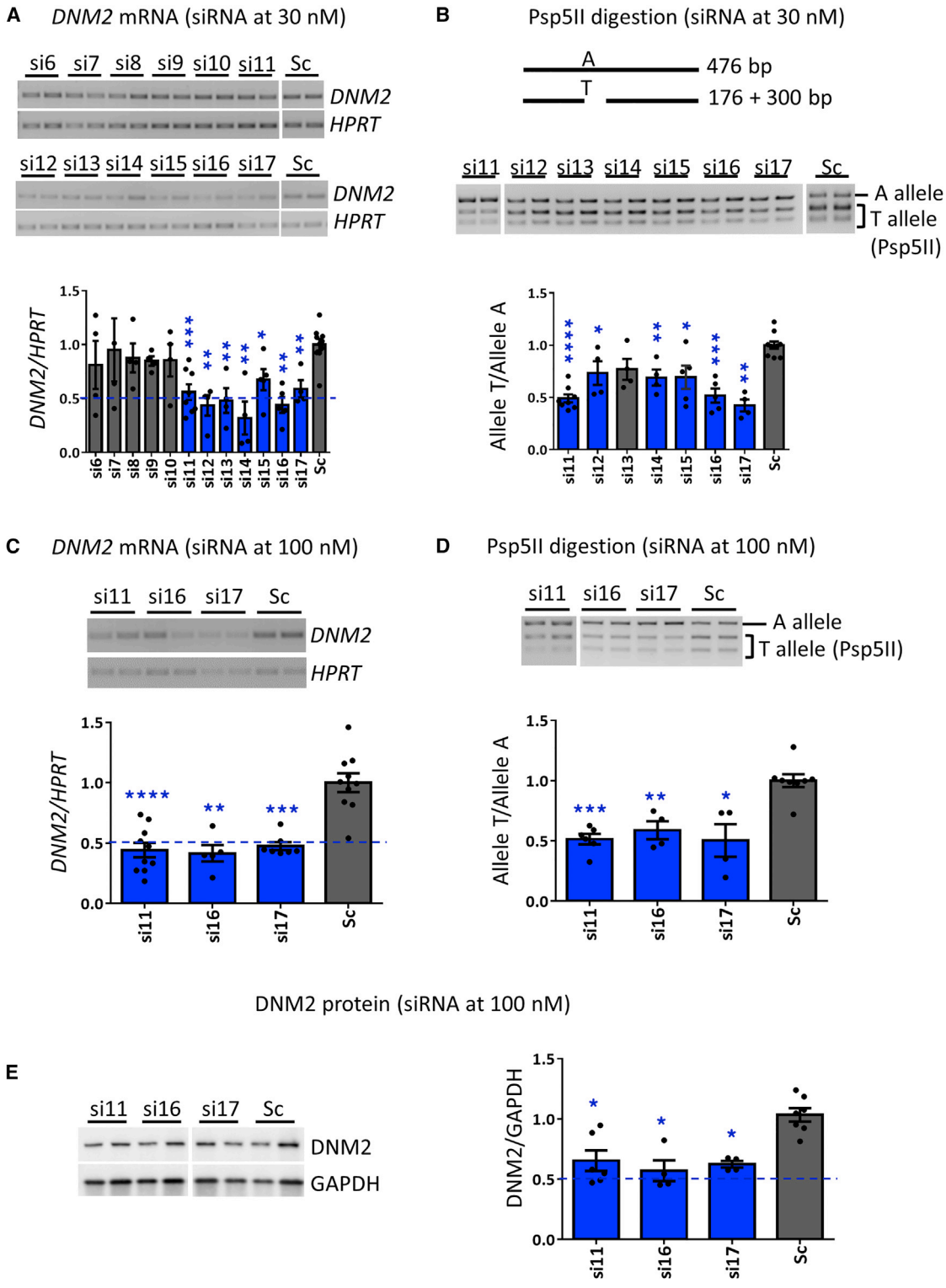

Figure 4. Identification of allele-specific siRNA against the T version of SNP2

(A) Expression of the *DNM2* mRNA 48 h after siRNA transfection at 30 nM. Agarose gel electrophoresis of *DNM2* and *HPRT* RT-PCR products and quantification of *DNM2* expression normalized to *HPRT* (n ≥ 4 per condition). (B) Psp5II digestion profile on the *DNM2* PCR product including the SNP2 sequence and quantification of the T/A ratio

(legend continued on next page)

mutation (R522H-fibroblasts) and increased in fibroblasts harboring the S619L mutation (S619L-fibroblasts) compared with control fibroblasts (Figure 7A), and western blot showed similar expression of transferrin receptor between control and mutant cells (Figure S8). Among the AS-siRNAs identified by our *in vitro* screening, we used si8 against the C version of the SNP1 (SNP1-si8-C, thereafter called siSNP1), si11 against the T version of the SNP2 (SNP2-si11-T, thereafter called siSNP2), and si10 against the p.S619L mutation (S619L-si10, thereafter called siS619) for the functional evaluation (Figure S7). The decrease in transferrin uptake noticed in R522H-fibroblasts was unchanged by siSNP1 and siSNP2 when transfected at 30 nM for 48 h (Figure 7B). At 100 nM, the values of transferrin uptake were increased by siSNP1 and siSNP2 close to the control values for siSNP1 after 48 h (Figure 7C). For the S619L-fibroblasts, the increase in transferrin was significantly reduced by siS619L and siSNP1 transfected at 30 nM, and this is maintained at 100 nM (Figures 7B and 7C).

By measuring the cell surface for transferrin uptake quantification, a defect was evidenced with a significantly smaller size for the R522H-fibroblasts and bigger size for the S619L-fibroblasts compared with the control cell line (Figure 7D). The impact of transfection of the three AS-siRNAs of interest was then evaluated on the cell-surface changes in patient-derived cells (Figures 7E and 7F). Among the tested AS-siRNAs, siSNP2 improved the cell size of the R522H-fibroblasts when transfected at 100 nM. For the S619L-fibroblasts, siSNP1 improved the cell size from 30 nM, and siS619L was able to restore cell size only when transfected at 100 nM. Overall, AS-siRNAs directed against non-pathogenic SNPs were found to be as effective as AS-siRNAs directly targeting the mutated nucleotide to restore CME and cell surface in patient-derived cells harboring two distinct *DNM2* mutations.

Rescue of cell migration by AS-siRNA

DNM2 dysfunction through its overexpression is known to promote cell migration, invasion, and metastasis in cancers.[12] Therefore, we looked for migration defects in the two fibroblast cell lines carrying the p.R522H and the p.S619L CNM mutations. We have tracked single cells during 24 h and compared the motility behavior in the two patient-derived cell lines and two healthy control cell lines. Both control cells present similar motility behavior (Figures 8A and S9A), but mutated fibroblasts presented cell motility defects, including a reduced mean speed (Figure 8A), an increased duration of pause, and a reduced speed when moving only for the S619L-fibroblasts (Figure S9A).

To assess the benefit of allele-specific siRNA, we performed the same experiment 48 h after cell transfection with either scramble siRNA or allele-specific siRNA (Figure S7). At the concentration of 30 nM, all measured parameters are impaired in mutant fibroblasts transfected with scramble siRNA compared with the control cell line transfected with a scramble. At this concentration, siSNP1 improved all impaired motility parameters in the R522H-fibroblasts (i.e., mean speed, number, and duration of pause and speed in motion). The siSNP2 fully rescued all the parameters at the control values (Figures 8B and S9B). For the S619L fibroblasts, siSNP1 and siS619L were effective to rescue or nearly rescue the motility parameters to the control values (Figures 8B and S9B). A second set of experiments was performed at 100 nM final concentration to evaluate the possibility of a full restoration of motility parameters for siSNP1 in the R522H cells. As shown in Figures 8C and S9C, 100 nM siSNP1 rescued all the motility parameters. Altogether these results highlight a decrease in cell motility associated with DNM2-CNM mutations that is restored using allele-specific siRNA.

Rescue of cell adhesion by AS-siRNA

The defects of both plasma membrane turnover caused by endocytosis impairment and cell migration evidenced in the *DNM2*-mutated cell lines (Figures 7 and 8) may also suggest an impact of the *DNM2* mutations on cell adhesion. We next assessed the adhesion capacity of the two CNM fibroblast cell lines by quantifying the number of adherent cells per square micrometer 1 h after seeding on glass coverslips. A decrease of cell density around 60% was measured in the S619L-fibroblasts compared with control, and no change occurred in the R522H-fibroblasts (Figure 8D). Consequently, we evaluated the impact of AS-siRNA transfected for 48 h only in S619L-fibroblasts. At 30 nM, siS619L and siSNP1 were unable to revert the adhesion defect (Figure 8E), whereas a partial rescue was achieved at 100 nM as intermediate values between patient-derived cells and healthy control cells values were measured (Figure 8F). Overall, these results showed that an adhesion defect may be present in CNM patient-derived cells, and that selected AS-siRNA against one SNP or the mutation similarly improve this phenotype.

DISCUSSION

Efficient silencing of morbid genes by RNAi has been at the origin of several clinical trials. Efficacy and specificity of RNAi were also used to specifically target the mutated allele in dominant inherited diseases as for the most frequent *DNM2* mutation causing CNM, which is due to a single-nucleotide change.[22] One bottleneck that may limit the development of therapy by AS-RNAi for the *DNM2*-linked CNM, and beyond for the other diseases linked to *DNM2* mutations, is the number of reported *DNM2* mutations and then the number of AS-siRNAs required to cover the entire patient population. Here, we addressed this key point for preclinical development of AS-RNAi therapy for AD-CNM by developing versatile AS-siRNA

($n \geq 4$ per condition) after transfection with siRNA at 30 nM. (C) Expression of the *DNM2* mRNA 48 h after siRNA transfection at 100 nM. Agarose gel electrophoresis of *DNM2* and *HPRT* RT-PCR products and quantification of *DNM2* expression normalized to *HPRT* ($n \geq 4$ per condition). (D) Psp5II digestion profile on the *DNM2* PCR product including the SNP2 sequence and quantification of the T/A ratio ($n \geq 4$ per condition) after transfection with siRNA at 100 nM. (E) DNM2 western blot and quantification of the signal by densitometry after siRNA transfection at 100 nM concentration. GAPDH was used as a loading control ($n \geq 4$). Data information: in scatterplots, the bars are mean values and error bars indicate SEM. ****$p < 0.0001$, ***$p < 0.001$, **$p < 0.01$ and *$p < 0.5$ using a two-tailed Mann-Whitney *U* test relative to the scramble siRNA (Sc).

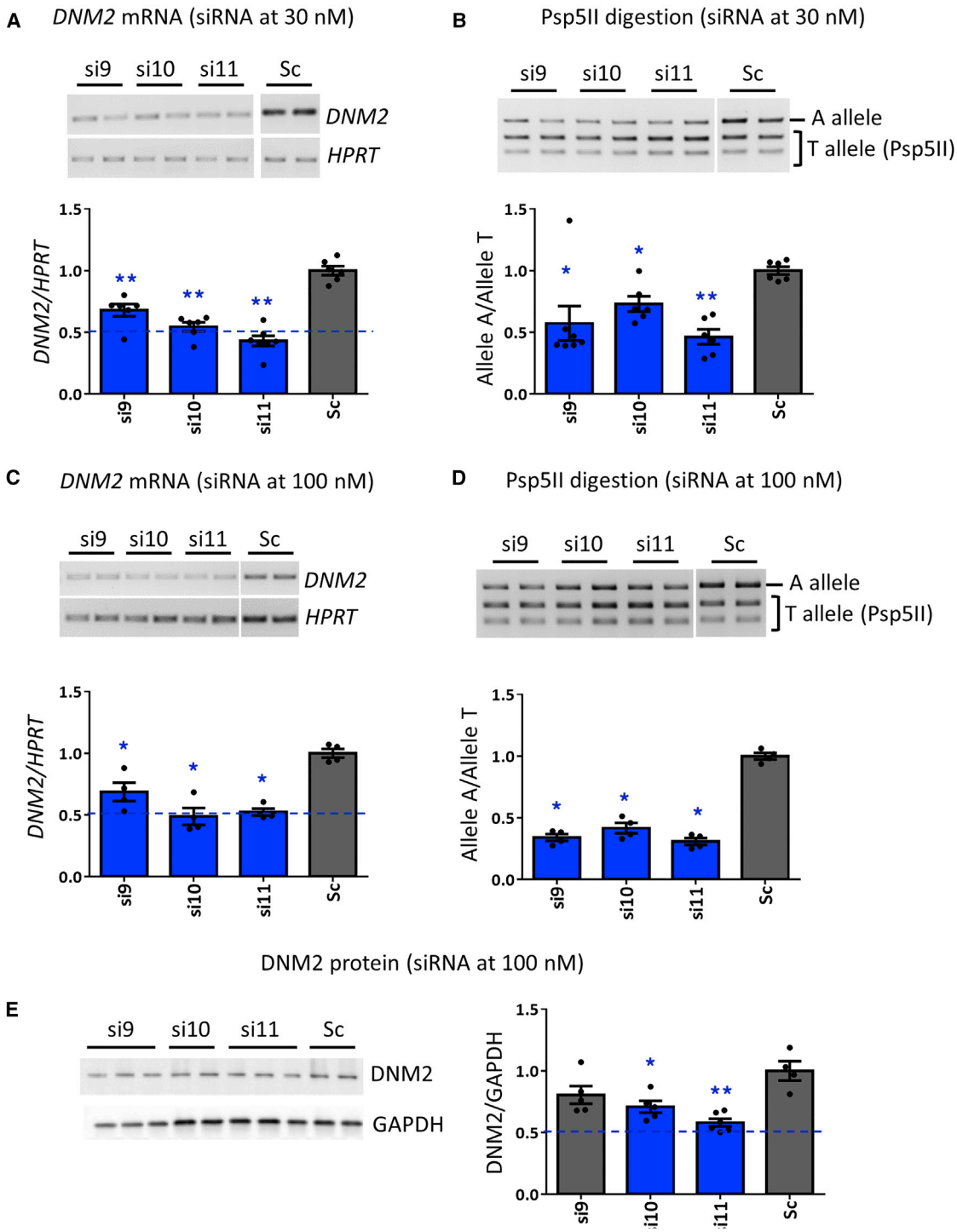

Figure 5. Identification of allele-specific siRNA against the A version of SNP2

(A) Expression of the *DNM2* mRNA 48 h after siRNA transfection at 30 nM. Agarose gel electrophoresis of *DNM2* and *HPRT* RT-PCR products and quantification of *DNM2* expression normalized to *HPRT* ($n \geq 4$ per condition). (B) Psp5II digestion profile on the *DNM2* PCR product including the SNP2 sequence and quantification of the A/T ratio ($n \geq 4$ per condition) after transfection with siRNA at 30 nM. (C) Expression of the *DNM2* mRNA 48 h after siRNA transfection at 100 nM. Agarose gel electrophoresis of *DNM2* and *HPRT* RT-PCR products and quantification of *DNM2* expression normalized to *HPRT* ($n \geq 4$ per condition). (D) Psp5II digestion profile on the *DNM2* PCR product including the SNP2 sequence and quantification of the A/T ratio ($n \geq 4$ per condition) after transfection with siRNA at 100 nM. (E) DNM2 western blot and quantification of the signal by densitometry after siRNA transfection at 100 nM concentration. GAPDH was used as a loading control ($n \geq 4$). Data information: in scatterplots, the bars are mean values and error bars indicate SEM. $^{**}p < 0.01$, $^{*}p < 0.5$ using a two-tailed Mann-Whitney *U* test relative to the scramble siRNA (Sc).

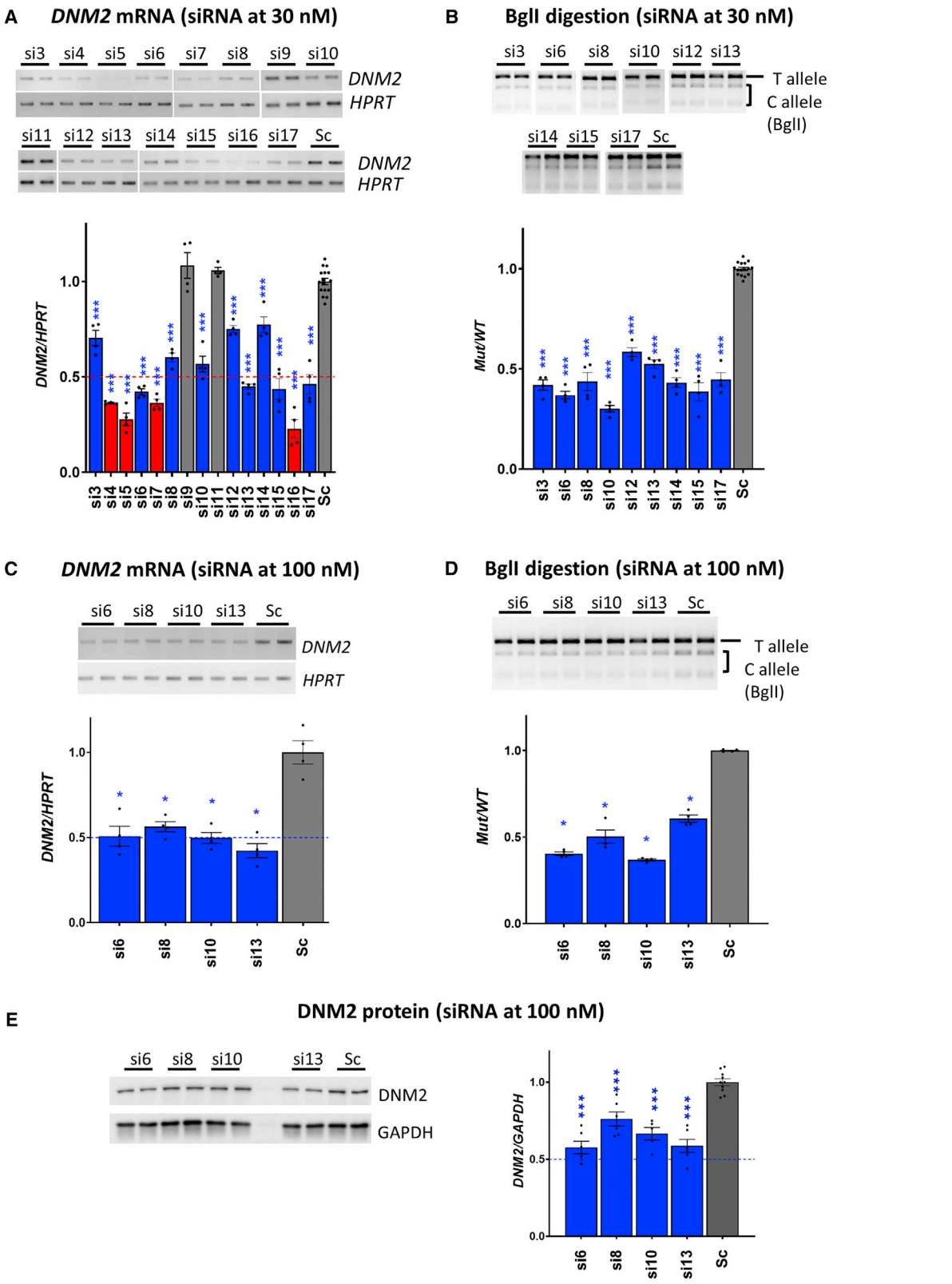

(legend on next page)

against two non-pathogenic SNPs displaying a wide spectrum of application for the *DNM2*-linked diseases.

Allele-specific siRNAs against SNP have been first developed in Huntington's disease[26–28,30,31] and spinocerebellar ataxia[27,32] because of the nature of the mutation, i.e., a repeated sequence also carried by the normal allele in a shorter version that makes it difficult to develop siRNA targeting directly the disease-associated sequence. For these diseases, the development of siRNAs benefited from the presence of SNPs linked to the mutations. There is no disease-associated SNP in the *DNM2*-linked dominant CNM, but the development of a similar strategy was made possible by the presence of two SNPs with a high frequency of heterozygosity (SNP1: 45% and SNP2: 30%). By this strategy, all the *DNM2* mutations can be silenced by choosing the siRNA against the version of the HTZ SNP carried by the mutated mRNA. Consequently, we developed efficient AS-siRNAs able to specifically silence each version of the two DNM2 SNPs. Relative to their frequency of heterozygosity in the population, siRNA against only these four targets allows covering ~60% of the AD-CNM patients. By adding the previously developed siRNA against the most frequent p.R645W mutation (27% of patients)[17] and the siRNA also developed in this study devoted to silencing the most frequent p.S619L mutation associated with the severe neonatal form of the disease (11% of patients),[17] ~75% of the AD-CNM population is covered.

One key step for the preclinical development of the AS-siRNA is the proof of principle for a therapeutic benefit in patient-derived cells using pertinent readout related to the CNM pathomechanisms. Past studies have given contradictory results concerning the effect of CNM-associated *DNM2* mutations on clathrin-dependent endocytosis, some showing a decrease,[18,29] others an absence of effect[33,34] or even an increase.[35] Despite these discrepancies, highlighting potential cell-type- and/or mutation-specific impacts, we evaluated this canonical role attributed to DNM2. As described previously,[18] we show that CME is impaired in patient fibroblasts and then may be used as a functional readout for evaluating allele-specific siRNA. Interestingly, our results point toward distinct impacts relative to the *DNM2* mutation because the R522H reduces endocytosis, whereas the S619L leads to increased endocytosis. We may hypothesize that these opposite impacts may participate in the diversity of the clinical spectrum associated with *DNM2* mutations. To identify additional readout, we took advantage of the growing number of studies showing the involvement of DNM2 dysfunction in the invasive behavior of cancer cells[10,11,36–43] to evaluate the migration of cells carrying CNM mutations. Indeed, DNM2 dysfunction induced by both R522H and S619L mutations similarly impairs patient-derived cells' migratory properties. In contrast, only the S619L mutation associated with the severe neonatal CNM form also impedes cell adhesion. Like for CME, the particular alteration of cell adhesion associated with the S619L mutation may start to highlight the cause of the clinical variability and especially the cause of the severe neonatal phenotype. Overall, our results represent a new argument in favor of impairment of the CME by CNM-*DNM2* mutations and highlight two new potential pathomechanisms through alteration of cell migration and adhesion. Further assessment will be required in a muscle context for a better characterization of the pathomechanisms in the DNM2-CNM because such migration and adhesion impairments may participate in the reduced muscle regeneration recently demonstrated in a mouse model of the disease.[44] In addition, this work allowed us to identify a panel of readouts for the functional evaluation of the AS-siRNA.

Functional evaluation was performed for the new AS-siRNA developed against the S619L mutation and the two SNPs. By this study, we showed that, except for adhesion, which is only partially restored, endocytosis, cell size, and cell migration are rescued by siS619 and siSNP1 in S619L-fibroblasts. In R522H-fibroblasts, endocytosis, size, and migration have been similarly partially or fully restored by the AS-siRNA against the two SNPs. Beyond the efficacy obtained for each AS-siRNA, this study demonstrates that a similar benefit is reached using a siRNA targeting a mutation or an SNP. In addition, results obtained in the R522H-fibroblasts show that siRNA developed against SNP1 located in the coding region and SNP2 located in the 3′ UTR are similarly efficient. However, regardless of the siRNA used, some defects are difficult to fully correct, as illustrated by adhesion impairment in the S619L cells. Such a highly integrated cell process may require a longer time to be restored. Nevertheless, the functional evaluation showed that all the allele-specific siRNAs developed against the S619L mutation and the two SNPs are largely efficient to rescue the defects identified in two patient-derived cell lines without inducing cell toxicity even at 100 nM.

Interestingly, the field of application of versatile siRNAs against SNPs goes far beyond the *DNM2*-linked CNM because these siRNAs may also be used for the other dominant diseases because of *DNM2* mutations, including dominant forms of the CMT and HSP. Due to the

Figure 6. Identification of allele-specific siRNA against the S619L DNM2 mutation

(A) Expression of the *DNM2* mRNA 48 h after siRNA transfection at 30 nM. Agarose gel electrophoresis of *DNM2* and *HPRT* RT-PCR products and quantification of *DNM2* expression normalized to *HPRT* ($n \geq 4$ per condition). (B) BglI digestion profile on the DNM2 PCR product including the SNP1 sequence and quantification of the mutant/WT ratio ($n \geq 4$ per condition) after transfection with siRNA at 30 nM. The mutant allele harbors the C version of SNP1. (C) Expression of the *DNM2* mRNA 48 h after siRNA transfection at 100 nM. Agarose gel electrophoresis of *DNM2* and *HPRT* RT-PCR products and quantification of *DNM2* expression normalized to *HPRT* ($n \geq 4$ per condition). (D) BglI digestion profile on the *DNM2* PCR product including the SNP1 sequence and quantification of the mutant/WT ratio ($n \geq 4$ per condition) after transfection with siRNA at 100 nM. (E) DNM2 western blot and quantification of the signal by densitometry after siRNA transfection at 100 nM concentration. GAPDH was used as a loading control ($n \geq 4$). Data information: in scatterplots, the bars are mean values and error bars indicate SEM. ***$p < 0.001$, *$p < 0.1$, using a two-tailed Mann-Whitney *U* test relative to the scramble siRNA (Sc).

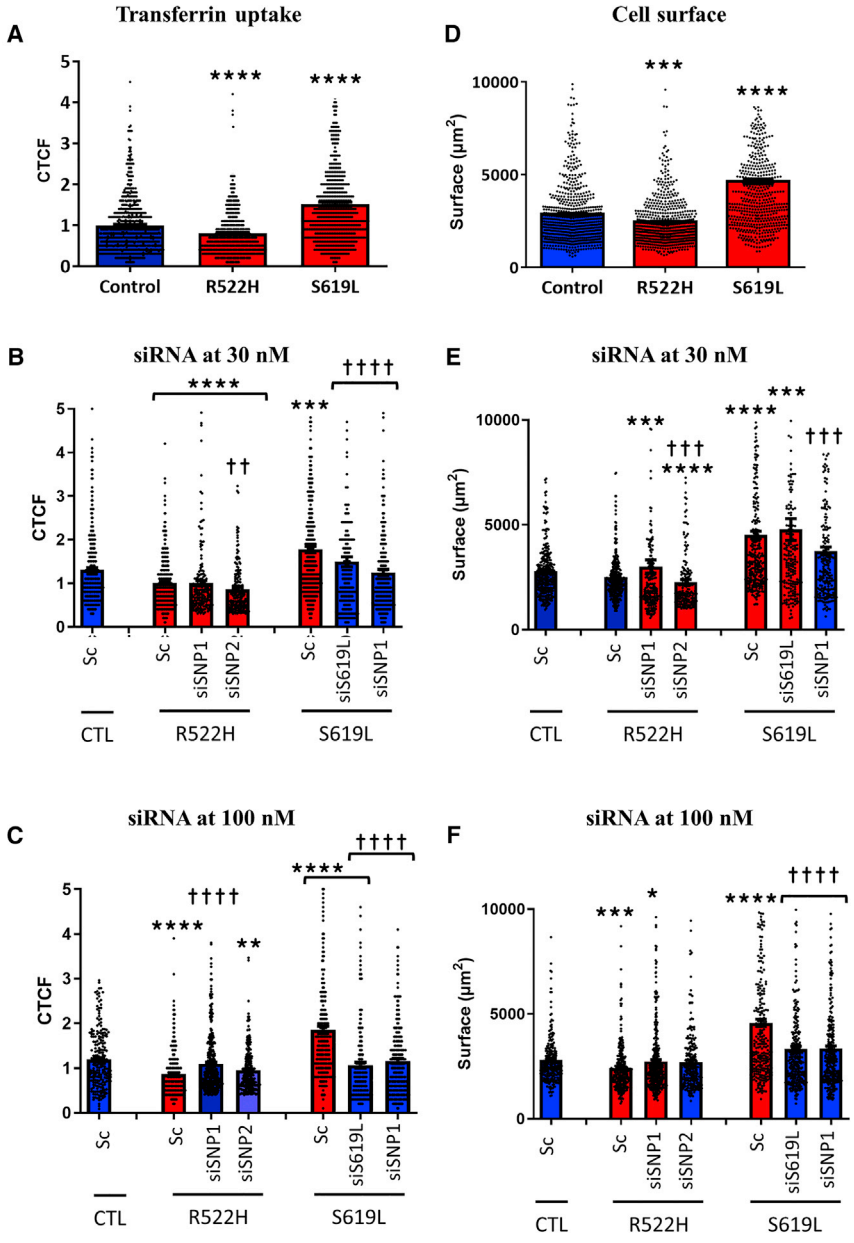

Figure 7. Impact of AS-siRNA on transferrin uptake and cell surface of patient-derived fibroblasts

(A) Transferrin uptake under basal conditions (n = 500–700 cells from three independent experiments). (B) Transferrin uptake after 48-h transfection with 30 nM scramble siRNA (Sc) or allele-specific siRNA against the S619L mutation or the two SNPs (n = 200–300 cells from two independent experiments). (C) Transferrin uptake after 48 h transfection with 100 nM Sc or allele-specific siRNA against the S619L mutation or the two SNPs (n = 200–300 cells from two independent experiments). (D) Cell surface (μm^2) under basal conditions (n = 500–700 cells from three independent experiments). (E) Cell surface after 48-h transfection with 30 nM Sc or allele-specific siRNA against the S619L mutation or the two SNPs (n = 200–300 cells from two independent experiments). (F) Cell surface after 48-h transfection with 100 nM Sc or allele-specific siRNA against the S619L mutation or the two SNPs (n = 200–300 cells from two independent experiments). Data information: bars represent mean values and error bars indicate SEM. Statistical analyses are performed using Kruskal-Wallis for (A)–(F) (****$p < 0.0001$ in all histograms), followed by Dunn's test relative to control cells in (A) and (D) (****$p < 0.0001$, ***$p < 0.001$ adjusted p value), control cells transfected with Sc in (B), (C), (E), and (F) (****$p < 0.0001$ adjusted p values), or the patient cell lines transfected with Sc in (B), (C), (E), and (F) ($^{\dagger}p < 0.05$, $^{\dagger\dagger}p < 0.01$, $^{\dagger\dagger\dagger\dagger}p < 0.0001$ adjusted p values). CTCF, corrected total cell fluorescence.

respective frequency of heterozygosity in humans, the development of the versatile siRNA may allow allele-specific silencing therapy in ~60% (according to frequency of heterozygosity reported in gnomAD) of the CMT and HSP patient population. The field of application of the versatile siRNAs is even wider because it also includes 60% of patients affected by diseases in which a deleterious overexpression of DNM2 has been reported, such as several cancers[12] and the X-linked recessive CNM.[13] The allele-specific siRNA developed in this study against the SNP may be used in these pathological conditions to reduce DNM2 expression in a controlled manner that avoids an excessive and potential toxic reduction below 50% by sparing one allele.

In conclusion, this study enriches the molecular toolbox with several novel allele-specific siRNAs directed against the most frequent *DNM2* mutation responsible for the severe neonatal dominant CNM and with versatile siRNA developed against two non-pathogenic SNPs able to target all the *DNM2* mutations. These new molecular tools also enlarge the number of patients eligible for the therapy by allele-specific DNM2 silencing by including diseases associated with either *DNM2* mutations or deleterious overexpression. The current proof of concept in patient-derived cells represents an important step for the preclinical development of this therapy for AD-CNM patients.

MATERIALS AND METHODS

Cell cultures and transfection

Healthy controls and CNM patient-derived fibroblast cell lines were obtained from the MyoLine platform for the immortalization of human cells (Institute of Myology, Paris, France) in accordance with European recommendations and French legislation (French Ministry of Higher Education and Scientific Research, approval no. AC-2013-1868). Written informed consent was obtained from all individuals and patients, prior to the study. Cell lines were cultured at

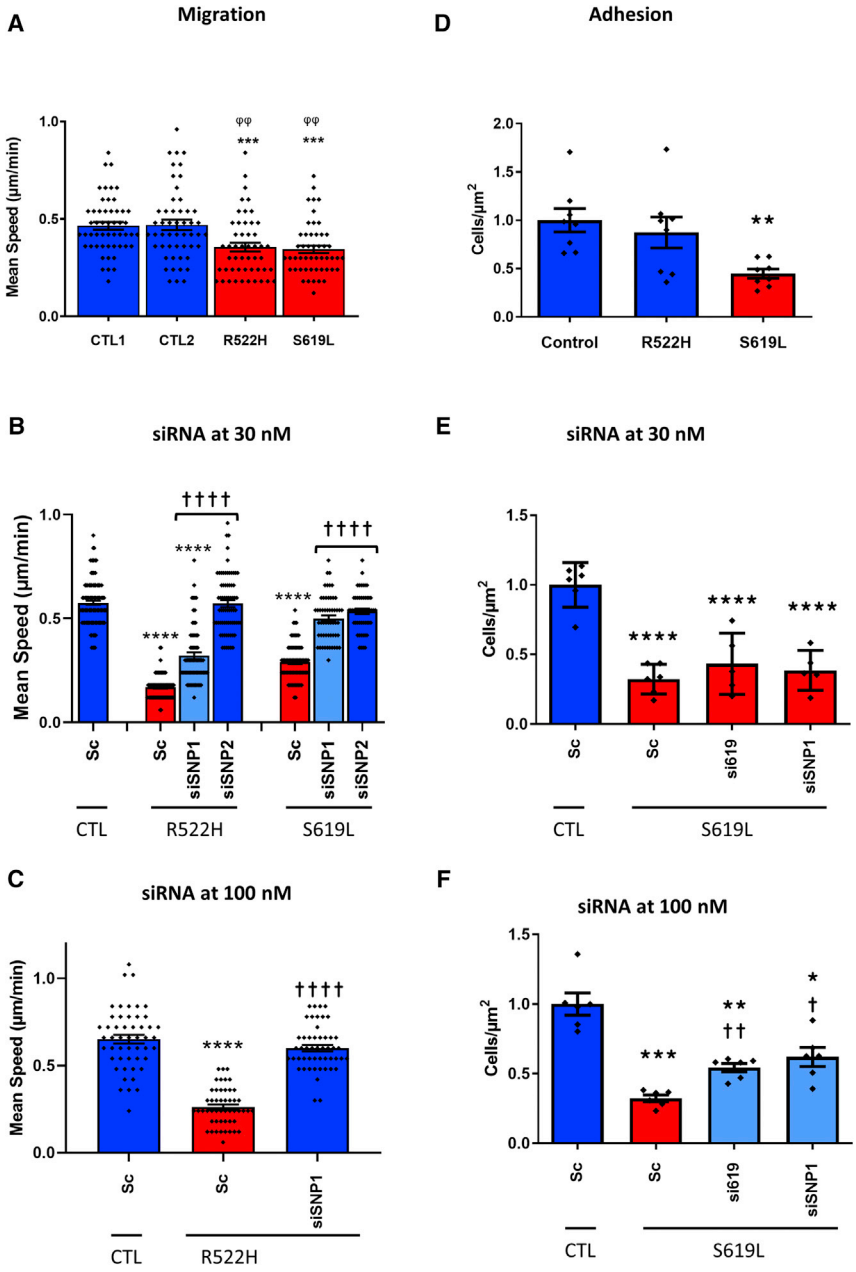

Figure 8. Migration and adhesion assays in patient-derived cells

(A) Mean speed of CNM and control fibroblasts (µm/min) under basal conditions (n = 50 cells tracked). (B) Mean speed of cells after 48-h transfection with 30 nM scramble siRNA (Sc) or allele-specific siRNA against the S619L mutation or the two SNPs (n = 50–70 cells tracked). (C) Mean speed of cells after 48-h transfection with 100 nM Sc or allele-specific siRNA against the SNP1 (n = 50–70 cells tracked). (D) Adhesion under basal conditions (n = 8 independent assays). (E) Adhesion assay after 48-h transfection with 30 nM Sc or allele-specific siRNA against the S619L mutation or the SNP1 (n = 5 or 6 independent transfections). (F) Adhesion assay after 48-h transfection with 100 nM Sc or allele-specific siRNA against the S619L mutation or SNP1 (n = 6 independent transfections). Data information: bars represent mean values and error bars indicate SEM. Statistical analyses are performed using Kruskal-Wallis for migration assay (A–C) (****$p < 0.0001$ in all histograms), followed by Dunn's test relative to control cells 1 (***$p < 0.001$) or control cells 2 ($^{\varphi\varphi}p < 0.01$) in (A), or to control cells transfected with Sc in (B) and (C) (****$p < 0.0001$), or to patient cell lines transfected with Sc in (B) and (C) ($^{\dagger\dagger\dagger\dagger}p < 0.0001$). ANOVA tests were performed for adhesion assay in (A) (**$p < 0.01$) and (B) and (C) (****$p < 0.0001$) followed by post-tests relative to control cells in (A) (**$p < 0.01$), to control cells transfected with Sc (****$p < 0.0001$, ***$p < 0.001$ **$p < 0.01$), and to patient cell lines transfected with Sc ($^{\dagger\dagger}p < 0.01$, $^{\dagger}p < 0.05$) in (B) and (C).

37°C (5% CO2) in Dulbecco's modified Eagle's medium (DMEM; Life Technologies, France) containing 10% fetal calf serum (FCS) supplemented with penicillin (100 U/mL) and streptomycin (100 µg/mL). Patient and control fibroblasts were immortalized using a lentiviral vector containing the sequence encoding the catalytic subunit of human telomerase (hTERT) as previously described.[45] For transfection, cells were grown to 70% confluency and transfected with siRNAs using RNAiMAX transfection reagent (Life Technologies, France) according to the manufacturer's protocol. The concentration of siRNAs for each experiment was indicated in corresponding figure legends. Allele-specific siRNA and scramble siRNA were purchased from Eurogentec (Belgium), and the sequences are available on request. Cells were used for functional evaluation or harvested for RNA and protein extraction 48 h after transfection.

Total RNA extraction and cDNA analysis

Total RNAs were isolated from cells using NucleoSpin RNA (Macherey-Nagel, France) according to the manufacturer's protocol. Cells were passed through a pipetting up-down several times for disruption in the lysis buffer. Total RNAs (500 ng) were submitted to reverse transcription using the Superscript III reverse transcriptase kit (Life Technologies, France) using oligo-dT primers in a final volume of 20 µL. Reverse transcription was performed at 50°C for 50 min, and a final step of 85°C for 5 min was added. To determine the allelic version of each SNP present on the mutated allele, PCR encompassing SNPs and the mutation was performed and cloned using the pGEMT vector system (Promega), and about 10 single clones were sequenced (Eurofins, France). The *DNM2* expression was quantified by semi-quantitative RT-PCR relative to the *HPRT* housekeeping gene expression. RT product (1 µL) was submitted to PCR performed at 96°C for 3 min followed by 27 cycles, including denaturation at 96°C for 25 s, annealing at 58°C for 25 s,

and polymerization at 72°C for 40 s, and a final step at 72°C for 5 min. The number of 27 PCR cycles has been selected to have the amplification in the exponential range for *DNM2* and *HPRT*. To quantify allele specificity of the assessed siRNA, we developed assays for SNP1 and SNP2 using restriction enzymes allowing discrimination between the two alleles after digestion of the RT-PCR products. PCR was designed to amplify regions of the *DNM2* transcript encompassing the SNPs. RT product (1 μL) was submitted to SNP1 or SNP2 PCR performed at 96°C for 3 min followed by 40 cycles, including denaturation at 96°C for 25 s, annealing at 58°C for 25 s, and polymerization at 72°C for 40 s, and a final step at 72°C for 5 min. The number of cycles has been selected to be at the end of the exponential phase of amplification. Ten microliters out of the 20 μL PCR products was digested overnight at 37°C using 7 units of BglI (New England Biolabs, France) for SNP1, and 15 μL out of the 30 μL PCR products was digested overnight at 37°C using 7 units of Psp5II (New England Biolabs, France) for SNP2. Image acquisition of the PCR products after agarose gel electrophoresis was performed using a Geni2 gel imaging system (Ozyme, France), and the associated signal was quantified using ImageJ Software (NIH; http://rsbweb.nih.gov/ij). All the PCR primers used in this study were from Eurogentec (Belgium), and sequences are available on request.

Protein extraction and western blot

Cell pellets were homogenized in lysis buffer containing 50 mM Tris-HCl (pH 7.5), 150 mM NaCl, 1% IGEPAL® CA-630, 0.5% deoxycholate sodium, and protease inhibitor cocktail 1% (Sigma--Aldrich, France) and kept on rotator for 20 min at 4°C. After cell lysates scraping, samples are lysed by sonication two times for 10 s at 30% of a maximum power of VCX 130 Vibra-cell ultrasonic processors (Sonics, USA). After centrifugation (12,000 × *g*, 4°C, 20 min), protein concentration in the supernatant was determined with the BCA Protein Assay Kit (Thermo Scientific Pierce, France). Five micrograms of proteins was mixed with a loading buffer (50 mM Tris-HCl, SDS 2%, glycerol 10%, β-mercaptoethanol 1%, and bromophenol blue) and denatured at 90°C for 5 min. Protein samples were separated on SDS-PAGE 10% pre-stained gels and transferred onto polyvinylidene fluoride (PVDF) membranes (0.45-μm pore size; Life Technologies, France) overnight at 100 mA at 4°C or nitrocellulose membranes (Bio-Rad Turbo transfer System) by *trans* blot at 25 V, 2.5 mA for 8 min. Membranes were blocked for 2 h at room temperature in PBS containing non-fat dry milk 5% and Tween 20 0.1% and then exposed to rabbit polyclonal anti-DNM2 antibody (ab3457 or ab65556; Abcam, France) or rabbit polyclonal anti-Transferrin receptor antibody (ab84036; Abcam, France) or rabbit polyclonal anti-GAPDH antibody (sc-25778; Santa Cruz, France) in PBS-Tween 20 0.1%, non-fat dry milk 1% overnight at 4°C. Membranes were rinsed in PBS-Tween 20 0.1% and incubated 2 h with horseradish peroxidase-conjugated secondary antibody (anti-rabbit from Jackson Immunoresearch, UK) in PBS-Tween 20 0.1%. Chemiluminescence was detected using ECL detection Kit (Merck-Millipore, Germany) in a Bio-Rad Chemidoc MP imaging system, and signal quantification was performed using ImageJ software.

Transferrin uptake assay and cell surface

Transfected cells were cultured in DMEM at 37°C for 45 min. Transferrin-Alexa Fluor 488 (Life Technologies, France) was added at 20 μg/mL at 37°C for 15 min. Cells were then washed in DMEM (pH 2) and PBS and fixed in paraformaldehyde 4% for 15 min. Image z stacks were acquired using an Axio Observer Apotome.2 microscope (Zeiss, Germany) using a 20× Plan Apochromat Zeiss objective. Individual cells were outlined manually on the sum projection of the confocal stacks to measure cell surface (μm^2), and the transferrin uptake was calculated using the ImageJ software for each cell according to the formula: corrected total cell fluorescence (CTCF) = integrated density of the cell − (mean fluorescence of background × cell area).

Adhesion assay

Cells were harvested by trypsinization 48 h after transfection or under basal conditions, and 35,000 cells were seeded on a 12-mm diameter glass coverslip in 24-well plates (three technical replicates for each transfection). After 1-h incubation at 37°C in DMEM-10%, FCS supplemented with penicillin (100 U/mL) and streptomycin (100 μg/mL), the non-attached cells were removed by PBS washing, and cells attached on coverslips were fixed in paraformaldehyde 4% for 15 min. Glass coverslips were mounted on slides with Vectashield medium (Vector Laboratories) containing DAPI to stain nuclei. Images were acquired using an Axio Observer Apotome.2 microscope (Zeiss, Germany) using a 2.5× Plan NeoFluar Zeiss objective, and the number of attached cells per square micrometer of coverslip was counted using ImageJ software through the counting of nuclei. Three independent experiments were done for each condition.

Cell tracking and analysis

Cells were seeded at low density on 24-well plastic plates under basal conditions or 48 h after transfection. Bright-field images were acquired at 10× magnification every 20 or 30 min (for transfected cells and basal condition, respectively) for 65 h using an inverted video-microscope equipped with heat and CO_2-controlled chamber (Nikon Ti2, Oko-Lab) driven by NIS (Nikon). After reconstruction of a 24-h movie, 50–70 cells per condition were randomly chosen and manually tracked by following the position of the nuclei using ImageJ software and MTrackJ plug-in to determine mean and maximum (max) speed.[46] Other motility parameters (mean speed in motion, number and duration of pause) were obtained using Skypad Microsoft Excel add-in that automatically analyzes particles in 2D trajectories.[47] A threshold of 10 μm was set out to consider the cell in movement between two time frames, and a speed threshold of 0.1 μm/min was set out to consider a relevant displacement.

Data analysis and statistics

Graphics and statistical analyses were performed with GraphPad Prism software versions 6 or 9 (GraphPad Software, La Jolla, CA, USA). Values were expressed as means ± SEM. The number of samples (n) represents the number of independent biological replicates, as indicated in the figure legends. The number of values analyzed, mean, and SEM for all the graphs presented in the figures are listed as Table S1.

We used non-parametric statistical tests to analyze our data when the normality could not be assumed (Shapiro-Wilk test) or tested (n too small). In this case, statistical comparisons between groups were performed using unpaired two-tailed Mann-Whitney *U* test for the siRNAs screening or using a Kruskal-Wallis test followed when significant by Dunn's for transferrin uptake, cell size, and migration assays. Adhesion assay was analyzed using ANOVA followed by Bonferroni post-test or Welch's ANOVA to correct the inequality of variance followed by Dunnett's as post-test. p values indicated for post hoc tests are adjusted p values; $p < 0.05$ was considered statistically significant.

Data availability statement

The authors confirm that all relevant data are included in the article and/or its supplemental information files.

SUPPLEMENTAL INFORMATION

Supplemental information can be found online at https://doi.org/10.1016/j.omtn.2022.08.016.

ACKNOWLEDGMENTS

We acknowledge the Platform for Immortalization of Human Cells at the Institut de Myologie (Paris, France) for the generation and distribution of the human cell lines. This work was supported by the Institut National de la Santé et de la Recherche Médicale (INSERM), Inserm Transfert (CoPoC grant), Association Institut de Myologie (AIM), Sorbonne Université, and Agence Nationale de la Recherche (ANR; Dynather, ANR-18-CE17-0006-02 to M.B.).

AUTHOR CONTRIBUTIONS

D.T. and M.B. conceived and designed the experiments. S.D., L.M., B.P., K.M., D.T., and M.B. performed the experiments. S.D., L.M., D.T., and M.B. analyzed the data. D.T. and M.B. wrote the manuscript.

DECLARATION OF INTERESTS

The authors declare no competing interests.

REFERENCES

1. Romero, N.B., and Bitoun, M. (2011). Centronuclear myopathies. Semin. Pediatr. Neurol. *18*, 250–256.
2. Hanisch, F., Muller, T., Dietz, A., Bitoun, M., Kress, W., Weis, J., Stoltenburg, G., and Zierz, S. (2011). Phenotype variability and histopathological findings in centronuclear myopathy due to DNM2 mutations. J. Neurol. *258*, 1085–1090.
3. Bitoun, M., Bevilacqua, J.A., Prudhon, B., Maugenre, S., Taratuto, A.L., Monges, S., Lubieniecki, F., Cances, C., Uro-Coste, E., Mayer, M., et al. (2007). Dynamin 2 mutations cause sporadic centronuclear myopathy with neonatal onset. Ann. Neurol. *62*, 666–670.
4. Bitoun, M., Maugenre, S., Jeannet, P.Y., Lacène, E., Ferrer, X., Laforêt, P., Martin, J.J., Laporte, J., Lochmuller, H., Beggs, A.H., et al. (2005). Mutations in dynamin 2 cause dominant Centronuclear Myopathy. Nat. Genet. *37*, 1207–1209.
5. Zuchner, S., Noureddine, M., Kennerson, M., Verhoeven, K., Claeys, K., De Jonghe, P., Merory, J., Oliveira, S.A., Speer, M.C., Stenger, J.E., et al. (2005). Mutations in the pleckstrin homology domain of dynamin 2 cause dominant intermediate Charcot-Marie-Tooth disease. Nat. Genet. *37*, 289–294.
6. Sambuughin, N., Goldfarb, L.G., Sivtseva, T.M., Davydova, T.K., Vladimirtsev, V.A., Osakovskiy, V.L., Danilova, A.P., Nikitina, R.S., Ylakhova, A.N., Diachkovskaya, M.P., et al. (2015). Adult-onset autosomal dominant spastic paraplegia linked to a GTPase-effector domain mutation of dynamin 2. BMC Neurol. *15*, 223.
7. Raja, S., Shah, S., Tariq, A., Bibi, N., Sughra, K., Yousuf, A., Khawaja, A., Nawaz, M., Mehmood, A., Khan, M., et al. (2019). Caveolin-1 and dynamin-2 overexpression is associated with the progression of bladder cancer. Oncol. Lett. *18*, 219–226.
8. Ren, N., Tian, Z., Sun, H., and Lu, X. (2020). Dynamin 2 is correlated with recurrence and poor prognosis of papillary thyroid cancer. Med. Sci. Monit. *26*, e924590.
9. Chernikova, S.B., Nguyen, R.B., Truong, J.T., Mello, S.S., Stafford, J.H., Hay, M.P., Olson, A., Solow-Cordero, D.E., Wood, D.J., Henry, S., et al. (2018). Dynamin impacts homology-directed repair and breast cancer response to chemotherapy. J. Clin. Invest. *128*, 5307–5321.
10. Eppinga, R.D., Krueger, E.W., Weller, S.G., Zhang, L., Cao, H., and McNiven, M.A. (2012). Increased expression of the large GTPase dynamin 2 potentiates metastatic migration and invasion of pancreatic ductal carcinoma. Oncogene *31*, 1228–1241.
11. Xu, B., Teng, L.H., Silva, S.D., Bijian, K., Al Bashir, S., Jie, S., Dolph, M., Alaoui-Jamali, M.A., and Bismar, T.A. (2014). The significance of dynamin 2 expression for prostate cancer progression, prognostication, and therapeutic targeting. Cancer Med. *3*, 14–24.
12. Trochet, D., and Bitoun, M. (2021). A review of Dynamin 2 involvement in cancers highlights a promising therapeutic target. J. Exp. Clin. Cancer Res. *40*, 238.
13. Cowling, B.S., Chevremont, T., Prokic, I., Kretz, C., Ferry, A., Coirault, C., Koutsopoulos, O., Laugel, V., Romero, N.B., and Laporte, J. (2014). Reducing dynamin 2 expression rescues X-linked centronuclear myopathy. J. Clin. Invest. *124*, 1350–1363.
14. Heymann, J.A., and Hinshaw, J.E. (2009). Dynamins at a glance. J. Cell Sci. *122*, 3427–3431.
15. Ferguson, S.M., and De Camilli, P. (2012). Dynamin, a membrane-remodelling GTPase. Nat. Rev. Mol. Cell Biol. *13*, 75–88.
16. Durieux, A.C., Prudhon, B., Guicheney, P., and Bitoun, M. (2010). Dynamin 2 and human diseases. J. Mol. Med. *88*, 339–350.
17. Bohm, J., Biancalana, V., Dechene, E.T., Bitoun, M., Pierson, C.R., Schaefer, E., Karasoy, H., Dempsey, M.A., Klein, F., Dondaine, N., et al. (2012). Mutation spectrum in the large GTPase dynamin 2, and genotype-phenotype correlation in autosomal dominant centronuclear myopathy. Hum. Mutat. *33*, 949–959.
18. Bitoun, M., Durieux, A.C., Prudhon, B., Bevilacqua, J.A., Herledan, A., Sakanyan, V., Urtizberea, A., Cartier, L., Romero, N.B., and Guicheney, P. (2009). Dynamin 2 mutations associated with human diseases impair clathrin-mediated receptor endocytosis. Hum. Mutat. *30*, 1419–1427.
19. Kenniston, J.A., and Lemmon, M.A. (2010). Dynamin GTPase regulation is altered by PH domain mutations found in centronuclear myopathy patients. EMBO J. *29*, 3054–3067.
20. Wang, L., Barylko, B., Byers, C., Ross, J.A., Jameson, D.M., and Albanesi, J.P. (2010). Dynamin 2 mutants linked to centronuclear myopathies form abnormally stable polymers. J. Biol. Chem. *285*, 22753–22757.
21. Ferguson, S., Raimondi, A., Paradise, S., Shen, H., Mesaki, K., Ferguson, A., Destaing, O., Ko, G., Takasaki, J., Cremona, O., et al. (2009). Coordinated actions of actin and BAR proteins upstream of dynamin at endocytic clathrin-coated pits. Dev. Cell *17*, 811–822.
22. Trochet, D., Prudhon, B., Beuvin, M., Peccate, C., Lorain, S., Julien, L., Benkhelifa-Ziyyat, S., Rabai, A., Mamchaoui, K., Ferry, A., et al. (2018). Allele-specific silencing therapy for Dynamin 2-related dominant centronuclear myopathy. EMBO Mol. Med. *10*, 239–253.
23. Trochet, D., Prudhon, B., Vassilopoulos, S., and Bitoun, M. (2015). Therapy for dominant inherited diseases by allele-specific RNA interference: successes and pitfalls. Curr. Gene Ther. *15*, 503–510.
24. Leachman, S.A., Hickerson, R.P., Schwartz, M.E., Bullough, E.E., Hutcherson, S.L., Boucher, K.M., Hansen, C.D., Eliason, M.J., Srivatsa, G.S., Kornbrust, D.J., et al. (2010). First-in-human mutation-targeted siRNA phase Ib trial of an inherited skin disorder. Mol. Ther. *18*, 442–446.

25. Golan, T., Khvalevsky, E.Z., Hubert, A., Gabai, R.M., Hen, N., Segal, A., Domb, A., Harari, G., David, E.B., Raskin, S., et al. (2015). RNAi therapy targeting KRAS in combination with chemotherapy for locally advanced pancreatic cancer patients. Oncotarget *6*, 24560–24570.

26. Lombardi, M.S., Jaspers, L., Spronkmans, C., Gellera, C., Taroni, F., Di Maria, E., Donato, S.D., and Kaemmerer, W.F. (2009). A majority of Huntington's disease patients may be treatable by individualized allele-specific RNA interference. Exp. Neurol. *217*, 312–319.

27. Fiszer, A., Olejniczak, M., Switonski, P.M., Wroblewska, J.P., Wisniewska-Kruk, J., Mykowska, A., and Krzyzosiak, W.J. (2012). An evaluation of oligonucleotide-based therapeutic strategies for polyQ diseases. BMC Mol. Biol. *13*, 6.

28. Takahashi, M., Watanabe, S., Murata, M., Furuya, H., Kanazawa, I., Wada, K., and Hohjoh, H. (2010). Tailor-made RNAi knockdown against triplet repeat disease-causing alleles. Proc. Natl. Acad. Sci. USA *107*, 21731–21736.

29. Ali, T., Bednarska, J., Vassilopoulos, S., Tran, M., Diakonov, I.A., Ziyadeh-Isleem, A., Guicheney, P., Gorelik, J., Korchev, Y.E., Reilly, M.M., et al. (2019). Correlative SICM-FCM reveals changes in morphology and kinetics of endocytic pits induced by disease-associated mutations in dynamin. FASEB J. *33*, 8504–8518.

30. van Bilsen, P.H., Jaspers, L., Lombardi, M.S., Odekerken, J.C., Burright, E.N., and Kaemmerer, W.F. (2008). Identification and allele-specific silencing of the mutant huntingtin allele in Huntington's disease patient-derived fibroblasts. Hum. Gene Ther. *19*, 710–719.

31. Drouet, V., Ruiz, M., Zala, D., Feyeux, M., Auregan, G., Cambon, K., Troquier, L., Carpentier, J., Aubert, S., Merienne, N., et al. (2014). Allele-specific silencing of mutant huntingtin in rodent brain and human stem cells. PLoS One *9*, e99341.

32. Scholefield, J., Watson, L., Smith, D., Greenberg, J., and Wood, M.J. (2014). Allele-specific silencing of mutant Ataxin-7 in SCA7 patient-derived fibroblasts. Eur. J. Hum. Genet. *22*, 1369–1375.

33. Liu, Y.W., Lukiyanchuk, V., and Schmid, S.L. (2011). Common membrane trafficking defects of disease-associated dynamin 2 mutations. Traffic *12*, 1620–1633.

34. Sidiropoulos, P.N., Miehe, M., Bock, T., Tinelli, E., Oertli, C.I., Kuner, R., Meijer, D., Wollscheid, B., Niemann, A., and Suter, U. (2012). Dynamin 2 mutations in Charcot-Marie-Tooth neuropathy highlight the importance of clathrin-mediated endocytosis in myelination. Brain *135*, 1395–1411.

35. Rabai, A., Reisser, L., Reina-San-Martin, B., Mamchaoui, K., Cowling, B.S., Nicot, A.-S., and Laporte, J. (2019). Allele-specific CRISPR/Cas9 correction of a heterozygous DNM2 mutation rescues centronuclear myopathy cell phenotypes. Mol. Ther. Nucleic Acids *16*, 246–256.

36. Burton, K.M., Cao, H., Chen, J., Qiang, L., Krueger, E.W., Johnson, K.M., Bamlet, W.R., Zhang, L., McNiven, M.A., and Razidlo, G.L. (2020). Dynamin 2 interacts with α-actinin 4 to drive tumor cell invasion. Mol. Biol. Cell *31*, 439–451.

37. Yamada, H., Takeda, T., Michiue, H., Abe, T., and Takei, K. (2016). Actin bundling by dynamin 2 and cortactin is implicated in cell migration by stabilizing filopodia in human non-small cell lung carcinoma cells. Int. J. Oncol. *49*, 877–886.

38. Zhang, Y., Nolan, M., Yamada, H., Watanabe, M., Nasu, Y., Takei, K., and Takeda, T. (2016). Dynamin2 GTPase contributes to invadopodia formation in invasive bladder cancer cells. Biochem. Biophys. Res. Commun. *480*, 409–414.

39. Razidlo, G.L., Wang, Y., Chen, J., Krueger, E.W., Billadeau, D.D., and McNiven, M.A. (2013). Dynamin 2 potentiates invasive migration of pancreatic tumor cells through stabilization of the Rac1 GEF Vav1. Dev. Cell *24*, 573–585.

40. Wong, B.S., Shea, D.J., Mistriotis, P., Tuntithavornwat, S., Law, R.A., Bieber, J.M., Zheng, L., and Konstantopoulos, K. (2019). A direct podocalyxin–dynamin-2 interaction regulates cytoskeletal dynamics to promote migration and metastasis in pancreatic cancer cells. Cancer Res. *79*, 2878–2891.

41. Yamada, H., Abe, T., Li, S.-A., Tago, S., Huang, P., Watanabe, M., Ikeda, S., Ogo, N., Asai, A., and Takei, K. (2014). N′-[4-(dipropylamino)benzylidene]-2-hydroxybenzohydrazide is a dynamin GTPase inhibitor that suppresses cancer cell migration and invasion by inhibiting actin polymerization. Biochem. Biophys. Res. Commun. *443*, 511–517.

42. Baldassarre, M., Pompeo, A., Beznoussenko, G., Castaldi, C., Cortellino, S., McNiven, M.A., Luini, A., and Buccione, R. (2003). Dynamin participates in focal extracellular matrix degradation by invasive cells. Mol. Biol. Cell *14*, 1074–1084.

43. Rosse, C., Lodillinsky, C., Fuhrmann, L., Nourieh, M., Monteiro, P., Irondelle, M., Lagoutte, E., Vacher, S., Waharte, F., Paul-Gilloteaux, P., et al. (2014). Control of MT1-MMP transport by atypical PKC during breast-cancer progression. Proc. Natl. Acad. Sci. USA *111*, E1872–E1879.

44. F Almeida, C., Bitoun, M., and Vainzof, M. (2021). Satellite cells deficiency and defective regeneration in dynamin 2-related centronuclear myopathy. FASEB J. *35*, e21346.

45. Auré, K., Mamchaoui, K., Frachon, P., Butler-Browne, G.S., Lombès, A., and Mouly, V. (2007). Impact on oxidative phosphorylation of immortalization with the telomerase gene. Neuromuscul. Disord. *17*, 368–375.

46. Meijering, E., Dzyubachyk, O., and Smal, I. (2012). Methods for cell and particle tracking. Methods Enzymol. *504*, 183–200.

47. Cadot, B., Gache, V., and Gomes, E.R. (2014). Fast, multi-dimensional and simultaneous kymograph-like particle dynamics (SkyPad) analysis. PLoS One *9*, e89073.